PHYSICAL REVIEW A **93**, 061401(R) (2016)

Inner-shell photoexcitations as probes of the molecular ions CH^+, OH^+, and SiH^+: Measurements and theory

J.-P. Mosnier,[1,*] E. T. Kennedy,[1] P. van Kampen,[1] D. Cubaynes,[2,3] S. Guilbaud,[2] N. Sisourat,[4] A. Puglisi,[4] S. Carniato,[4] and J.-M. Bizau[2,3]

[1]*School of Physical Sciences and NCPST, Dublin City University, Dublin 9, Ireland*

[2]*Institut des Sciences Moléculaires d'Orsay, CNRS, Université Paris–Sud, and Université Paris-Saclay, F-91405 Orsay, France*

[3]*Synchrotron SOLEIL, L'Orme des Merisiers, Saint-Aubin, BP 48, F-91192 Gif-sur-Yvette Cedex, France*

[4]*Laboratoire de Chimie Physique-Matière et Rayonnement, Université Pierre et Marie Curie, 11 Rue Pierre et Marie Curie, 75231 Paris Cedex 05, France*

(Received 15 October 2015; published 14 June 2016)

Spectral probes for the CH^+, OH^+, and SiH^+ hydride molecular ions that play key roles in astrophysics and plasma processes are presented. The merged-beam technique at the SOLEIL synchrotron was used to record the photoionization (ion yield) spectra of CH^+, OH^+, and SiH^+ and that of their parent atomic ions, in the K-shell and L-shell regions, respectively. Energies and oscillator strengths for the $K\alpha$ (CH^+ and OH^+) and $L\alpha$ (SiH^+) transitions were determined from the spectra. *Ab initio* calculations interpret the experimental data in terms of contributions from ground and excited valence electronic states.

DOI: 10.1103/PhysRevA.93.061401

Inner-shell photoionization in neutral or ionized atoms and molecules immersed in an x-ray (0.1–10 keV) background radiation field produce atomic species and molecular fragments with increased ionization and chemical reactivity via Auger emission and highly excited states and thus play determining roles in shaping species abundance and the dynamics of large-scale gaseous systems. Examples include laboratory high-density laser plasmas [1], the hot plasmas of stellar coronae [2], and the interstellar clouds and protoplanetary disks of star-forming regions [3–5]. The latter are important molecular regions where collisions with abundant hydrogen produce molecular hydride species and their ions, e.g., OH^+ [6]. Enhanced hydride abundance and chemical activity result when the molecular gas is exposed to x rays from the star, in x-ray dissociation regions, driving chemical evolution [7]. The interpretation of the experimental spectra and the modeling of the physical or chemical properties of these complex systems require laboratory measurements of the relevant photoabsorption or ionization and photodissociation reaction cross sections [8,9]. These are important not only to benchmark theoretical calculations of the fundamental reaction rates, but also to provide unique identification of atomic and molecular species and their relative abundances [10].

There has been ongoing progress in developing experimental (at dedicated third-generation synchrotron radiation facilities), theoretical, and computational approaches to understand the photon cross-section behavior of core-excited atomic ions [11], encapsulated atoms and ions [12], and neutral molecules [13]. In this work we tackle the corresponding challenge in the case of core-excited molecular ions. The reduced number of valence electrons in a molecular ion, compared to the neutral, leads to increased Coulomb forces and a different interplay with the chemical forces during the electronic (Auger processes) and nuclear (dissociation processes) relaxations of the core-excited species. A systematic study of such effects is one of the primary motivators for our work. Photoionization studies in molecular ions are still in their infancy in spite of their long-standing importance in astrophysics [14] or plasma applications [15]. There is the notable exception of the CO^+ ion for which absolute photoionization cross sections in the valence regime were obtained using the photon-ion merged-beam technique [16]. This technique was also used to show the collective excitation of valence electrons (surface and volume plasmons) in the absolute photoionization cross sections of the C_{60}^+, C_{60}^+, and C_{60}^+ molecular ions [17] and recently in an investigation of the relative cross sections for the photoionization of $Lu_3N@C_{80}^+$ endohedral fullerene molecular ions at photon energies near the carbon K edge [18]. Related works on the photofragmentation pathways of the HeH^+ molecular ion [19] and $H^+(H_2O)_2$ solvated protons [20] were carried out using VUV pulses from the FLASH free-electron laser.

In this Rapid Communication we report the short-wavelength photoabsorption cross-section spectra of the key hydride CH^+, OH^+ (K-shell regions), and SiH^+ (L-shell region) molecular ions and provide their analyses with the help of *ab initio* theoretical calculations. Our exemplars were selected for their importance in both astronomical and various laboratory environments. CH^+ (methylidyne) is ubiquitous in molecular clouds and questions of the formation and abundance of interstellar CH^+ remain outstanding problems in molecular astrophysics [21]. It also plays important roles in magnetic fusion plasmas [22], reducing hydrocarbon plasmas for diamondlike carbon layer deposition [23] and carbon nanocone processing [24]. Interstellar OH^+ (oxoniumylidene) has been detected recently [25] and is a key ion in the oxygen chemical network leading to the formation of water and other important precursor molecules in the interstellar medium [26]. Photoionization of the related molecular systems OH [27] and H_3O^+ [28] has been recently studied. The production of H_nO^+ ions is important in the plasma processing of metallic surfaces [29] and the treatment of organic wastes [30]. Silicon-based molecules are significant trace constituents in late-type stars and star-forming regions, representing nearly 10% of the molecular species identified in space [31]. SiH^+ (silylidyne)

*Corresponding author: jean-paul.mosnier@dcu.ie

is isoelectronic with AlH and chemically similar to CH^+; its solar oscillator strength and photodissociation in interstellar clouds and stellar atmospheres have been investigated below the 13.6-eV Lyman limit [32]. Thin-film silicon and solar cell technologies use plasma-enhanced chemical vapor deposition reactors with silane (SiH_4) as the process gas. The roles played by the $SiH_n (n = 1–3)$ silane radicals and molecular ions have long been recognized as key to optimizing the reactor growth regime to tailor thin-film material properties [33].

The CH^+ and $OH^+ K\alpha$ photon energies reported here constitute reference data for the interpretation of the photon energy shifts due to chemical environment or interactions, often sought in soft-x-ray probe techniques near the C and O K edges. Examples of such techniques include soft-x-ray cryotomography, scanning transmission x-ray microscopy, cryoelectron microscopy, and x-ray-absorption near-edge structure for the study of radiation chemistry [34], radiation damage [35], submicron resolution three-dimensional biological imaging [36], and amino-acid adsorption on carbon nanotubes [37]. Furthermore, as we estimate the molecular hydride cross sections from ion-yield data and a comparison with those of the parent atomic ions (C^+, O^+, and Si^+) measured in absolute terms on the same apparatus, our results are also relevant to the understanding of the inverse formation or association mechanism for the CH^+, OH^+, and SiH^+ molecular ions [14].

The experiments were performed with the photon-ion merged-beam setup installed on one branch of the PLEIADES beamline at the synchrotron facility SOLEIL [38]. The CH^+, OH^+, and SiH^+ hydride ions were produced in a permanent magnet electron cyclotron resonance (ECR) ion source by heating methane (CH_4), water (H_2O), and silane (SiH_4) gases, respectively, with a 12.6-GHz microwave generator. To extract the ions, a 4-kV bias was applied to the source and charge to mass separation of the ions was achieved using a 90° dipole magnet. After collimation by two sets of slits, the selected ions were merged with the monochromatized photon beam in the interaction region. The latter is 50 cm long and terminates with a circular aperture of 2 cm diameter, which determines the solid angle of acceptance for detection of the fragmentation channels. After the aperture, an einzel lens refocuses the transmitted ions to the detector. The ion current in this region is of the order of 50 nA for the CH^+ and SiH^+ ions and 550 nA for OH^+. The synchrotron radiation emitted in the HU80 undulator is monochromatized by a high-flux 600-line/mm plane grating. The photon flux is systematically monitored using a calibrated Si photodiode. Photon energies are determined using a double-ionization gas cell of the Samson type [39] and corrected for the Doppler shift resulting from the velocity of the parent ions.

We have analyzed our experimental spectra with the help of *ab initio* calculations of the CH^+, OH^+, and SiH^+ molecular energy-level structures and the $1s \rightarrow n\pi$ and $2p \rightarrow n\delta$ transition moments, respectively. Only the salient features of the calculations are provided here. The potential energy and dipole moment surfaces were computed using the configuration-interaction single (CIS) method. For the OH^+ and CH^+ ions, the relaxation effects upon K-shell core-hole creation were large and taken into account by choosing the restricted open-shell Hartree-Fock reference wave function with a hole in the $1s$ orbital. Spin-orbit effects were small and were neglected. For the SiH^+ system, core relaxation effects were taken into account by fixing the core hole in the $2s$ rather than the $2p$ subshell in order to avoid the effects of a preferential direction due to one of the three $2p_{x,y,z}$ directional orbitals. Comparable relaxation effects are expected for the $2s$ and $2p$ levels, which are energetically close. Spin-orbit coupling in the Si $2p^{-1}$ H^+ core-excited states is significant and is included through the full Breit-Pauli operator. For the calculations, an aug-cc-pvQz basis set [40] was used and $7s$, $6p$, $5d$, and $3f$ diffuse functions were included for the excited element (C, O, or Si) to improve the description of the spectrum in the Rydberg region. All the computations were performed with the GAMESS-US package [41]. A diagrammatic representation explaining the various steps leading to the evaluation of the dipole transition moment from the electronic ground state to the jth core-hole excited electronic state is given in Ref. [42]. Because of the high computational cost of the spin-orbit coupling calculation step, we approximated the potential energy curve using a second-order Taylor expansion. Franck-Condon profiles were computed using standard wave-packet methods [43]: For each core-excited electronic state the initial nuclear wave function multiplied by the dipole transition moment was propagated on the potential energy surface from which the autocorrelation function was obtained. The absorption spectrum was then obtained by a Fourier transform of the autocorrelation function. Literature values of about 6 fs (109 meV) [44], 4 fs (160 meV) [44], and 15 fs (45 meV) [45] were used respectively for the CH^+, OH^+, and SiH^+ core-hole lifetimes. The wave packet was propagated for more than four times the core-hole lifetime to ensure convergence of the absorption spectra. A more detailed description of the theoretical treatment is beyond the scope of the present paper.

The CH^+, OH^+, and SiH^+ cross sections, measured with an experimental bandpass (BP) of 280, 200, and 80 meV, respectively, are presented as a function of the photon energy in the top panels of Figs. 1, 2, and 3. Cross-section (Mb) scales for these spectra were obtained by assuming equal cross-section values for the parent atomic (see below) and hydride species in the high-energy photon range above the thresholds for direct K- or L-shell ionization. The spectra represent the sole contribution of the signals measured in the doubly ionized C^{2+}, O^{2+}, and Si^{2+} fragmentation channels, respectively. No significant contributions from the C^+, O^+, Si^+, and H^+ singly ionized or any triply ionized decay fragments were observed. In the photon range close to the K- and L-shell energies, the $AH^+ + h\nu \rightarrow A^{2+} + H + \bar{e}$ (where A = C, O, or Si and $\bar{e}$ represents a free electron in the continuum) photodissociation processes therefore appear dominant, although the $AH^+ + h\nu \rightarrow A^+ + H^+ + \bar{e}$ decay route cannot be ruled out.

In our experimental conditions, the detection of ionized species, and H^+ in particular, is made more difficult as a result of reduced detection efficiency arising from both the species angular spread associated with fragmentation lateral momentum effects [46] and collisional background noise. As the deflection angle is greatest for the largest lateral velocity of the fragmentation ion, the geometrical collection efficiency is thus lowest (greatest) for fragmentations occurring early

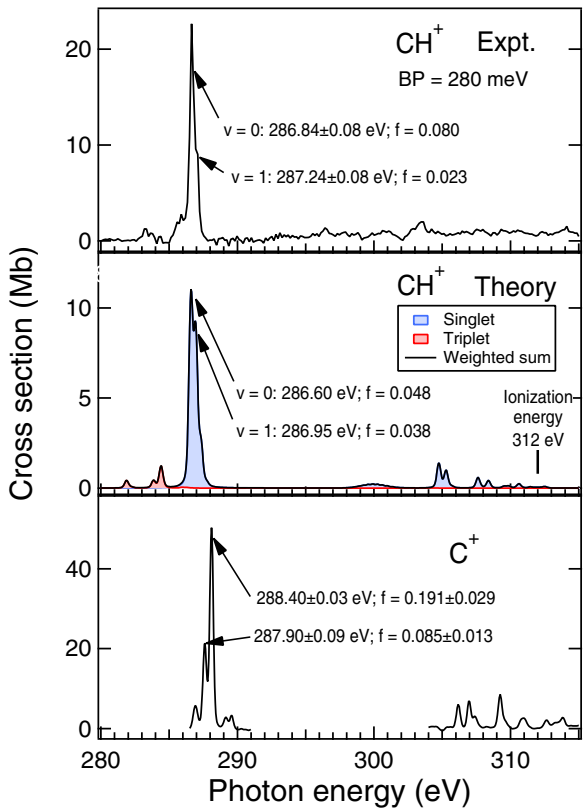

FIG. 1. Experimental (top) and theoretical (middle) photoionization cross-section spectra of the CH^+ molecular ion and experimental photoionization cross-section spectrum (bottom) of the C^+ atomic ion, in the carbon K-edge region. The measured and calculated (*ab initio* values shifted by 3 eV) photon energies and oscillator strengths (f value) of the main $X\,^1\Sigma \rightarrow {}^1\Pi(v = 0,1)$ inner-shell resonance are shown.

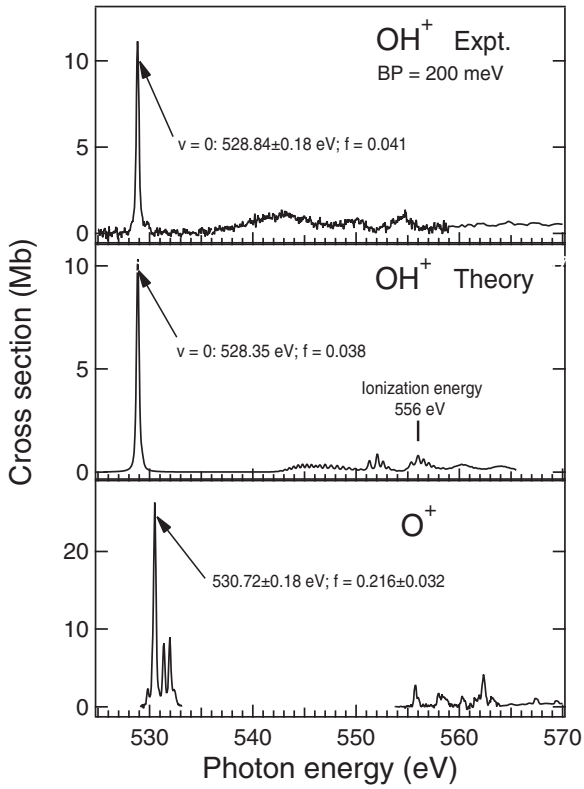

FIG. 2. Experimental (top) and theoretical (middle panel) photoionization cross-section spectra of the OH^+ molecular ion and experimental photoionization cross-section spectrum (bottom) of the O^+ atomic ion, in the oxygen K-edge region. The measured and calculated (*ab initio* values shifted by 0.5 eV) photon energies and oscillator strengths (f value) of the main inner-shell $X\,^3\Sigma \rightarrow {}^3\Pi$ resonance are shown.

(late) in the interaction region. Application of momentum and energy conservation laws provides insight into the geometrical collection efficiency constraints. For example, a 10-eV kinetic energy release upon fragmentation for the CH^+ core-excited molecule would result in a 3.5-$\mathrm{km\,s^{-1}}$ maximum lateral velocity of the carbon atomic ion, producing a corresponding maximum lateral deflection of about 7 mm at the exit plane. This is well within the limits of the collection geometry described above and all the C^{2+} fragments released with kinetic energies up to 10 eV lie within the collection solid angle, no matter where along the interaction region the fragmentation occurs. For the same fragmentation, the hydrogen lateral deflection would be ∼90 mm and very few H^+ ions would be detected, particularly against a noisy background. The maximum values of the kinetic energy release (KER) constrained by the aperture-defined solid angle for fragmentation of core excited CH^+, OH^+, and SiH^+ occurring at the beginning of the interaction zone are ∼20, 26, and 45 eV, respectively. For KER values less than these limits, all heavy-ion fragments lie within the collection solid angle.

We have carried out first calculations of the CH^{2+} lowest-potential-energy curves using the methods described above. Under the assumption that fragmentation begins with the molecule at equilibrium internuclear distance and zero kinetic energy, the calculations showed KER values below 20 eV for all the states populated after Auger decay. Owing to their larger equilibrium internuclear distance, KER values lying in a lower range are expected for OH^+ and SiH^+. These findings, taken together with literature data on measured KER values upon dissociation of other small core-excited or ionized molecules [13,28,47], suggest that the collection efficiencies for the doubly ionized C, O, and Si channel species are effectively uncompromized by the acceptance solid angle. This is in sharp contrast to the lighter H^+ ions, which during fragmentation take away the majority of the kinetic energy due to the large C, O, and Si/H mass ratios.

The middle panels of the figures show the calculated cross-section spectra after convolution with a Gaussian function of width (full width at half maximum) equal to the experimental BP. For comparison with the experimental data (top panels) the computed spectra were globally shifted in energy to match the most intense resonances. The computations also included contributions due to $1s$ or $2p$ inner-shell excitation from low-lying valence excited metastable electronic states, necessary for the interpretation of the CH^+ and SiH^+ spectra. The general agreement in terms of the overall shape between the theoretical and experimental spectra is satisfactory for all three cases. However, a comparison of experimental and theoretical values for the cross sections, integrated to

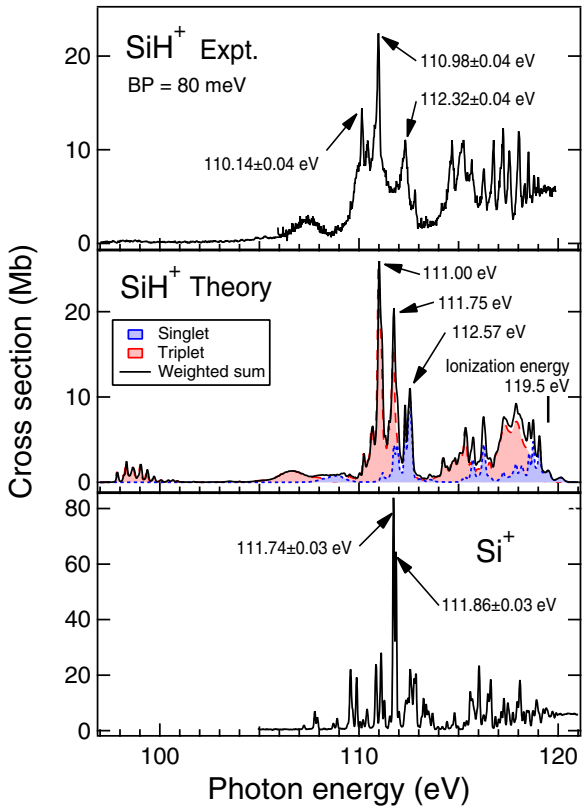

FIG. 3. Experimental (top) and theoretical (middle) (with *ab initio* energies shifted by 2.5 eV) photoionization cross-section spectra of the SiH^+ molecular ion and experimental photoionization cross-section spectrum (bottom) of the Si^+ atomic ion, in the silicon L-edge region.

the ionization threshold (see the top and middle panels of Figs. 1–3), shows that significant differences remain in terms of absolute values. The corresponding [expt. (theor.)] integrated cross-section values are for CH^+ [29.4 (11.7)], OH^+ [18.2 (10.0)], and SiH^+ [69.9 (51.6)] Mb eV. The experimental and theoretical discrepancies may be partly explained by the current computational limitations of our CIS approach. In the calculations both the initial and the single-core-excited states are represented as configuration-interaction (CI) expansions of Slater determinants. Due to both the large size of the CI matrix and the huge number of states, we have restricted the expansions to include singly excited determinants only. The inclusion of more determinants, notably those representing doubly excited configurations, would further improve the calculations but would require computational power greater than currently available.

The bottom panels present the absolute cross sections for the C^+, O^+, and Si^+ atomic ions, respectively, in the K-shell and L-shell regions. These were measured in this work from the total ion-yield signal, viz., the sum of the dominant single- and double-ionization channels, with the same experimental BP as for their molecular hydride counterpart, applying a 1-kV bias on the 50-cm-long tube defining the interaction region. The top spectrum of each figure can be interestingly viewed as the effect on the inner-shell photoionization of the atomic C^+, O^+, and Si^+ ions due to the bonding of a hydrogen atom to form the molecular CH^+, OH^+, and SiH^+ ions.

The CH^+ spectrum features a sharp and intense resonance, centered at 287.0-eV photon energy, with an underlying vibrational structure, the details of which are given in the top panel of Fig. 1. Weak and broad structures are also observed between 295 and 320 eV and on the low-energy side of the 287.0-eV resonance. The latter structures are attributed to $1s$ inner-shell excitations from the CH^+ valence excited electronic state $a\,^3\Pi$ at 1.14 eV [48] above the singlet CH^+ ground state. This triplet state is likely to be produced in the ECR source and travel to the photon interaction zone due to its metastable character. The weak structures are adequately reproduced in the synthetic spectrum of the middle panel of Fig. 1 if it comprises 90% and 10% contributions from the $K(2s\sigma)^2(2p\sigma)^2\,X\,^1\Sigma^+$ ground and metastable $a\,^3\Pi$ states, respectively. The primary photon excitation mechanism for the strongest resonance corresponds to the $K(2s\sigma)^2(2p\sigma)^2X\,^1\Sigma^+ \rightarrow (1s\sigma)(2s\sigma)^2(2p\sigma)^2(2p\pi)\,^1\Pi$ dipole absorption process, i.e., a $1s \rightarrow 2p\pi$ inner-shell excitation. This is the molecular counterpart of the $1s \rightarrow 2p$ excitations in atomic C^+ [49] shown in the bottom panel around 288 eV: The similarity between the two spectra in this narrow region is evident. The energy of the K-shell excited molecular ion is ultimately given off through electron emission in resonant Auger decay and molecular dissociation processes with the final products of the reaction being measured as $C^{2+}(1s^22s^2\,^1S_0) + H(1s\,^2S_{1/2}) + \bar{e}$. The $1s \rightarrow 2p\pi$ resonance is reproduced satisfactorily in the theoretical spectrum. Its fine structure can be understood in terms of the vibrational profile ($v = 0$ and 1 distribution) of the core-excited potential energy surface. The corresponding oscillator strengths corrected for the populations of the initial states have been extracted from both the experimental and theoretical spectra and are seen to compare reasonably well (see Fig. 1). Above 300 eV the theoretical spectrum predicts cross-section behavior in the form of Rydberg series converging on the CH^+ K-shell ionization energy calculated at 312 eV. The experimental cross sections in this region show distinct shallow modulations reaching values of about 1 Mb around 303.7 eV.

The OH^+ spectrum is expectedly similar to CH^+ (see Fig. 2). It is dominated by a strong resonance at 528.84 eV corresponding to $1s \rightarrow 2p\pi$ ($v = 0$) excitations in the ground electronic state $K(2s\sigma)^2(2p\sigma)^2(2p\pi)^2X\,^3\Sigma^-$ of OH^+. Higher $1s \rightarrow np\sigma,\pi$ excitations to empty molecular orbitals give broad and weak structures with maxima at 543.2, 549.7, and 554.5 eV. The agreement between the calculated results and the experimental data is seen to be very satisfactory for the 528.84-eV resonance; see also the oscillator strength values of Fig. 2. The $X\,^3\Sigma^-$ ground-state calculations without any contributions from valence-excited electronic states were sufficient to explain the major features of the observed OH^+ spectrum. The OH^+ inner-shell excited $(1s\sigma)(2s\sigma)^2(2p\sigma)^2(2p\pi)^3\,^3\Pi$ electronic state ultimately decays primarily to doubly ionized atomic oxygen via resonant Auger decay and molecular dissociation to the $O^{2+}(1s^22s^22p^2\,^3P) + H(1s) + \bar{e}$ final products. The patterns of the weak cross-section structure between 540 and 560 eV are seen to be satisfactorily reproduced by the calculations. The broad structure between 535 and 548 eV is due to the dissociative character of the inner-shell excited electronic states. The ionization energy of the K shell in OH^+ is calculated at 556 eV. The $1s$ spectrum of O^+ [50] obtained

with the same setup is shown in the bottom panel of Fig. 2 and a comparison with the top panel indicates the effect of chemical bond formation between O^+ and H. Similarly to CH^+, it results in a shift towards lower energy and a strong reduction of the oscillator strength of the $1s \rightarrow 2p\pi$ resonance.

SiH^+ is chemically analogous to CH^+ and its electronic ground-state configuration is $KL(3s\sigma)^2(3p\sigma)^2X\ ^1\Sigma^+$. The first valence excited electronic state ($a\ ^3\Pi$) lies 2.29 eV above the ground state [51]. The main structure of the experimental spectrum observed in the 106–113 eV arises from the excitation of an atomiclike $2p$ electron of the type $2p_{1/2,3/2} \rightarrow 3d\sigma,\pi,\delta$ to empty molecular-orbital states (see Fig. 3). The $L_{II,III}$ spin-orbit splitting of silicon is of the order of 0.7 eV [52] and results in a fine structure of the molecular bands. The observed structure can only be satisfactorily interpreted if contributions due to inner-shell excitations from the $a\ ^3\Pi$ triplet state are added to the ground-state cross sections. As shown in Fig. 3, reasonable agreement is achieved between the theoretical and experimental spectra if the synthetic spectrum includes a 50% fraction of the $a\ ^3\Pi$ state. Above 114 eV up to about 120-eV photon energies, the $2p$ inner-shell excitations to highly excited molecular states form characteristic Rydberg series converging on the $L_{II,III}$ ionization limits calculated at 119.5 eV. Here again, based on experimental evidence, the resonant Auger decay of the SiH^+ L-shell excited states and dissociation result in doubly ionized silicon $Si^{2+}(1s^22s^22p^63s^2\ ^1S) + H(1s) + \bar{e}$.

In conclusion, we have measured inner-shell excitations for molecular ions and their parent atomic ions by using the same ECR plasma molecular ion source coupled with monochromatized synchrotron radiation in a merged-beam configuration. The energies and photoexcitation cross sections of the main resonances in the inner-shell spectra of germane molecular hydride ions, namely, the K-shell spectra of CH^+ and OH^+ and the L-shell spectrum of SiH^+, were measured. Through *ab initio* theoretical calculations, based on the configuration-interaction single approach, we have shown that interpretation of the spectra requires consideration of both ground- and valence-excited electronic-state contributions. The experimental and theoretical data will enable identification of these molecules in astronomical sources and laboratory plasmas and will also aid the modeling of the species abundance and dynamics. Our investigations of three distinct molecular ions, together with their parent atomic ions, underpin the versatility of the merged-beam technique and suggest that rapid progress should be possible in the largely unexplored field of the inner-shell photoionization of molecular ions.

The authors wish to thank the PLEIADES beam staff, for help during the experiments, and the European Commission (FP7), the Agence Nationale de la Recherche (Programme Investissements d'Avenir Grant No. ANR-11-IDEX-0004-02), and the LABEX Plas@Par consortium, for financial assistance.

[1] J. L. Kline *et al.*, Phys. Rev. Lett. **106**, 085003 (2011).
[2] A. R. Foster, R. K. Smith, N. S. Brickhouse, T. R. Kallman, and M. C. Witthoeft, Space Sci. Rev. **157**, 135 (2010); T. R. Kallman and P. Palmeri, Rev. Mod. Phys. **79**, 79 (2007).
[3] P. Stäuber, S. D. Doty, E. F. van Dishoek, and A. O. Benz, Astron. Astrophys. **440**, 949 (2005).
[4] M. Àdàmkovics, A. E. Glassglod, and R. Meijerink, Astrophys. J. **736**, 143 (2011).
[5] S. Lepp and A. Dalgarno, Astron. Astrophys. **306**, L21 (1996).
[6] A. G. G. M. Tielens, Rev. Mod. Phys. **85**, 1021 (2013).
[7] A. O. Benz *et al.*, Astron. Astrophys. **521**, L35 (2010); M. Ádámkovics, A. E. Glassgold, and J. R. Najita, Astrophys. J. **786**, 135 (2014); J. R. Najita, M. Ádámkovics, and A. E. Glassgold, *ibid.* **743**, 147 (2011); S. Hirose and N. J. Turner, Astrophys. J. Lett. **732**, L30 (2011).
[8] E. Gatuzz, J. García, T. R. Kallman, C. Mendoza, and T. W. Gorczyca. Astrophys. J. **800**, 29 (2015); W. C. Stolte, V. Jonauskas, D. W. Lindle, M. M. Sant'Anna, and D. W. Savin, *ibid.* **818**, 149 (2016).
[9] D. W. Savin *et al.*, Rep. Prog. Phys. **75**, 036901 (2012).
[10] T. Ryabchikova and L. Mashonkina, Phys. Scr. **89**, 114007 (2014).
[11] D. A. Macaluso, A. Aguilar, A. L. D. Kilcoyne, E. C. Red, R. C. Bilodeau, R. A. Phaneuf, N. C. Sterlin, and B. M. McLaughlin, Phys. Rev. A **92**, 063424 (2015); E. T. Kennedy, J.-P. Mosnier, P. Van Kampen, D. Cubaynes, S. Guilbaud, C. Blancard, B. M. McLaughlin, and J.-M. Bizau, *ibid.* **90**, 063409 (2014).
[12] A. Müller, S. Schippers, M. Habibi, D. Esteves, J. C. Wang, R. A. Phaneuf, A. L. D. Kilcoyne, A. Aguilar, and L. Dunsch, Phys. Rev. Lett. **101**, 133001 (2008); A. L. D. Kilcoyne *et al.*, *ibid.* **105**, 213001 (2010).
[13] J. D. Bozek and C. Miron, J. Electron. Spectrosc. Rel. Phenom. **204**, 269 (2015); S. L. Sorensen, Eur. Phys. J. Spec. Top. **169**, 79 (2009); K. Ueda, J. Phys. Soc. Jpn. **75**, 032001 (2006); I. Nenner and P. Morin, in *VUV and Soft X-Ray Photoionization*, edited by U. Becker and D. A. Shirley (Plenum, New York, 1996), p. 291.
[14] C. Sánchez Contreras *et al.*, Astron. Astrophys. **577**, A52 (2015); W. D. Geppert and M. Larsson, Chem. Rev. **113**, 8872 (2013); M. Alagia *et al.*, Rend. Lincei **24**, 53 (2013); W. D. Langer, Astrophys. J. **225**, 860 (1978).
[15] Y. Ju and W. Sun, Prog. Energ. Combust. **48**, 21 (2015); N. S. Shuman, D. E. Hunton, and A. A. Viggiano, Chem. Rev. **115**, 4542 (2015).
[16] T. Andersen, H. Kjeldsen, H. Knuden, and F. Folkmann, J. Phys. B **34**, L327 (2001); G. Hinojosa *et al.*, Phys. Rev. A **66**, 032718 (2002).
[17] S. W. J. Scully *et al.*, Phys. Rev. Lett. **94**, 065503 (2005).
[18] J. Hellhund, A. Borovik, Jr., K. Holste, S. Klumpp, M. Martins, S. Ricz, S. Schippers, and A. Müller, Phys. Rev. A **92**, 013413 (2015).
[19] H. B. Pedersen *et al.*, Phys. Rev. Lett. **98**, 223202 (2007).
[20] L. Lammich *et al.*, Phys. Rev. Lett. **105**, 253003 (2010).
[21] S. Bovino, T. Grassi, and F.A. Gianturco, J. Phys. Chem. A **119**, 11973 (2015); E. F. Van Dishoeck, in *The Molecular*

Astrophysics of Stars and Galaxies, edited by T. W. Harquist and D. A. Williams, International Series on Astronomy and Astrophysics Vol. 4 (Clarendon, Oxford, 1998), p. 85.

[22] R. K. Janev and D. Reiter, Phys. Plasmas **9**, 4071 (2002).

[23] W. Ensinger, Surf. Coat. Technol. **203**, 772 (2009).

[24] S. Mehrabian, S. Xu, A. A. Qaemi, B. Shokri, and K. Ostrikov, Phys. Plasmas **20**, 033501 (2013).

[25] F. Wyrowski, K. M. Menten, R. Güsten, and A. Belloche, Astron. Astrophys. **518**, A26 (2010).

[26] D. Hollenbach, M. J. Kaufman, D. Neufeld, M. Wolfire, and J. R. Goicoechea, Astrophys. J. **754**, 105 (2012); A. J. Porras, S. R. Federman, D. E. Welty, and A. M. Ritchey, Astrophys. J. Lett. **781**, L8 (2014); N. Indriolo *et al.*, Astrophys. J. **800**, 40 (2015); E. González-Alfonso *et al.*, Astron. Astrophys. **550**, A25 (2013).

[27] S. Stranges, R. Richter, and M. Alagia, J. Chem. Phys. **116**, 3676 (2002).

[28] H. B. Pedersen *et al.*, Phys. Rev. A **80**, 012707 (2009); C. Domesle, S. Dziarzhytski, N. Guerassimova, L. S. Harbo, O. Heber, L. Lammich, B. Jordon-Thaden, R. Treusch, A. Wolf, and H. B. Pedersen, *ibid.* **88**, 043405 (2013).

[29] L. Pranevicius, L. L. Pranevicius, P. Vilkinis, S. Baltaragis, and K. Gedvilas, Appl. Surf. Sci. **295**, 240 (2014).

[30] G. Ling, Plasma Sci. Technol. **16**, 223 (2014).

[31] M. C. McCarthy, C. A. Gottlieb, and P. Thaddeus, Mol. Phys. **101**, 697 (2003).

[32] P. C. Stancil, K. Kirby, A. B. Sannigrahi, R. J. Buenker, G. Hirsch, and J.-P. Gu, Astrophys. J. **486**, 574 (1997).

[33] T. Roschek, T. Repmann, J. Müller, B. Rech, and H. Wagner, J. Vac. Sci. Technol. A **20**, 492 (2002); S. G. Sayres, M. W. Ross, and A. W. Castleman, Jr., Phys. Rev. A **82**, 033424 (2010); P. B. Davies and P. M. Martineau, J. Chem Phys. **88**, 485 (1988).

[34] M. A. Aronova, A. A. Sousa, and R. D. Leapman, Micron **42**, 252 (2011).

[35] A. F. G. Leontowich, A. P. Hitchcock, and R. F. Egerton, J. Electron. Spectrosc. Relat. Phenom. **206**, 58 (2016).

[36] R. Carzaniga, M.-C. Domart, L. M. Collinson, and E. Duke, Protoplasma **251**, 449 (2014).

[37] J. Zhong *et al.*, Mater. Lett. **63**, 431 (2009).

[38] J. M. Bizau *et al.*, J. Electron. Spectrosc. Relat. Phenom. **210**, 5 (2016); C. Miron, C. Nicolas, and E. Robert, http://www.synchrotronsoleil.fr/Recherche/LignesLumiere/PLEIADES

[39] J. A. R. Samson, *Techniques of Vacuum Ultraviolet Spectroscopy* (Wiley, New York, 1967).

[40] D. E. Woon and T. H. Dunning, Jr., J. Chem. Phys. **98**, 1358 (1993).

[41] M. W. Schmidt *et al.*, J. Comput. Chem. **14**, 1347 (1993).

[42] E. Kawerk *et al.*, J. Electron Spectrosc. **186**, 1 (2013).

[43] E. J. Heller, Acc. Chem. Res. **14**, 368 (1981); D. J. Tannor, *Introduction to Quantum Mechanics: A Time Dependent Perspective* (University Science Press, Sausalito, 2007).

[44] C. Nicolas and C. Miron, J. Electron Spectrosc. Relat. Phenom. **185**, 267 (2012).

[45] J. D. Bozek, G. M. Bancroft, J. N. Cutler, and K. H. Tan, Phys. Rev. Lett. **65**, 2757 (1990).

[46] G. Hinojosa, M. M. Sant'Anna, A. M. Covington, R. A. Phaneuf, I. R. Covington, I. Domínguez, A. S. Schlachter, I. Alvarez, and C. Cisneros, J. Phys. B **38**, 2701 (2005).

[47] T. A. Carlsonn and M. O. Krause, J. Chem. Phys. **56**, 3206 (1972); A. P. Hitchcock, P. Lablanquie, P. Morin, E. Lizon A. Lugrin, M. Simon, P. Thiry, and I. Nenner, Phys. Rev. A **37**, 2448 (1988); D. Mathur, E. Krishnakumar, K. Nagesha, V. R. Marathe, V. Krishnamurti, F. A. Rajgara, and U. T. Raheja, J. Phys. B **26**, L141 (1993).

[48] K. P. Huber and G. Herzberg, *Molecular Spectra and Molecular Structure, IV. Constants of Diatomic Molecules* (Springer, New York, 1979).

[49] A. Müller *et al.*, Phys. Rev. Lett. **114**, 013002 (2015).

[50] J. M. Bizau, D. Cubaynes, S. Guilbaud, M. M. Al Shorman, M. F. Gharaibeh, I. Q. Ababneh, C. Blancard, and B. M. McLaughlin, Phys. Rev. A **92**, 023401 (2015).

[51] A. B. Sannigrahi, R. J. Buenker, G. Hirsch, and J. P. Gu, Chem. Phys. Lett. **237**, 204 (1995).

[52] W. Hayes and F. C. Brown, Phys. Rev. A **6**, 21 (1972).